IEEE Access
Multidisciplinary | Rapid Review | Open Access Journal

Received 13 January 2024, accepted 26 January 2024, date of publication 7 February 2024, date of current version 20 February 2024.

Digital Object Identifier 10.1109/ACCESS.2024.3363440

RESEARCH ARTICLE

Boundary Value Controlled Gamma Z-Source Inverter for Pump Applications

KRISHNAN SELVARAJ[1], G. D. ANBARASI JEBASELVI[2], MOHAMMED H. ALSHARIF[3], AND MUN-KYEOM KIM[4]

[1]Department of Electrical and Electronics Engineering, Sathyabama Institute of Science and Technology, Chennai 600119, India
[2]Department of Electronics and Communication Engineering, Sathyabama Institute of Science and Technology, Chennai 600119, India
[3]Department of Electrical Engineering, College of Electronics and Information Engineering, Sejong University, Seoul 05006, Republic of Korea
[4]School of Energy Systems Engineering, Chung-Ang University, Dongjak-gu, Seoul 06974, Republic of Korea

Corresponding authors: Krishnan Selvaraj (krishna05me@gmail.com) and Mun-Kyeom Kim (mkim@cau.ac.kr)

This work was supported by the Basic Science Research Program through the National Research Foundation of Korea (NRF) funded by the Ministry of Education under Grant 2020R1A2C1004743.

ABSTRACT This work presents a solution for controlling an Asynchronous Motor Drive (AMD) using a Gamma Z Source Inverter (GZSI) in combination with a high-gain Quadratic Boost Converter (QBC). The higher voltage gain of QBC and GZSI reduces the voltage rating of PV. Reduced output voltage ripple of QBC improves the performance of the AMD system. The proposed PV-QBC-GZSI-AMD system aims to regulate the motor's speed for applications requiring a constant speed. The approach involves implementing a closed-loop control system and evaluating different controllers: Current-mode-Fractional Order Proportional Integral (CM-FOPI), Current-mode-Proportional Resonant (CM-PR), and Current Mode-Hysteresis Controller (CM-HC). Also, FOPI improves the robustness and the hysteretic controller reduces the current-ripple implemented in this model. Hence, the system's performance is assessed using MATLAB/Simulink, showcasing enhanced dynamic performance in speed and torque characteristics within the time domain when employing CM-FOPI, CM-PR, and CM-HC control strategies for PV-QBC-GZSI-AMD. Simulation outcomes are compared against actual motor speed and torque data, highlighting the superior performance of the closed-loop-CM-HC control in PV-QBC-GZSI-AMD over closed-loop-CM-FOPI and CM-PR methods. Closed-loop-CM-HC control also provides over current protection. The study also includes hardware results from the PV-QBC-GZSI-AMD system, validating the simulation findings. Furthermore, the performance of the proposed converter topology is compared with notable existing works, considering essential factors such as the number of stages, loops, control method, load type, performance parameters, and associated limitations.

INDEX TERMS GZSI- Gamma Z-source inverter, HC- hysteresis controller, PR-proportional resonant, QBC-quadratic boost converter, AMD- asynchronous motor drive, CM- current mode, FOPI-fractional order PI.

I. INTRODUCTION

A. BACKGROUND

Power electronic converters are essential components in modern pump systems as they provide precise control over the speed and torque of the motor, leading to increased efficiency and energy savings [1], [2]. As a result, there has been a growing interest in the application of various converter topologies to pump systems to achieve higher efficiency, reliability, and cost-effectiveness [3], [4]. Several studies have been conducted to investigate the application of different converter topologies in pump systems, such as the Z-Source inverter [5], the Quasi-Z-Source inverter [6], the Matrix converter [7], and the PWM inverter [8]. These studies have shown promising results in terms of system efficiency, power quality, and energy savings. However, each

The associate editor coordinating the review of this manuscript and approving it for publication was Akshay Kumar Saha.

converter topology has its advantages and disadvantages, and the performance of the converter is highly dependent on the application requirements. Therefore, a comprehensive evaluation of the different converter topologies in pump systems is essential to determine the optimal solution for a particular application. A z-source inverter is a type of power inverter, a circuit that converts direct current to alternating current. The circuit functions as a buck-boost inverter without making use of a DC-DC converter bridge due to its topology.

Impedance (Z) source networks efficiently convert power between source and load from DC to DC, DC to AC, and from AC to AC. The number of modifications and new Z-source topologies has grown rapidly since 2002. Improvements to the impedance networks by introducing coupled magnetics have also been lately proposed for achieving even higher voltage boosting while using a shorter shoot-through time. They include the Γ-source, T-source, trans-Z-source, TZ-source, and LCCT-Z-source that utilizes a high-frequency transformer connected in series with two DC-current-blocking capacitors.

The Quasi Z-Source Buck-Boost (QBC) inverter, a modified version of the traditional Z-Source inverter, has emerged as a promising option for pump applications. QBC inverter can boost the voltage of low input voltage sources and provide bidirectional power flow, making it suitable for various pump applications. Several studies have investigated the application of QBC-fed Z-Source inverters in pump systems. For instance, in [9], a QBC-fed Z-Source inverter was designed and implemented for a water pump system, showing superior performance compared to traditional inverters. Similarly, in [6], a QBC-fed Z-Source inverter was used for a solar-powered pump system, resulting in improved energy efficiency and cost-effectiveness. Overall, the application of QBC-fed Z-Source inverters in pump systems has shown promising results, with significant improvements in system efficiency, power quality, and energy savings.

B. LITERATURE SURVEY

Pumps are commonly used in various industrial and residential applications such as water supply, irrigation, heating, ventilation, and air conditioning (HVAC) systems. The efficiency and performance of the pump system is influenced by the type of motor and control technique used. The traditional approach for controlling pumps is to use the direct-on-line (DOL) starting method, which has limited efficiency and may cause damage to the pump motor. Hence, there is a need for more advanced control methods and efficient motor drives for pump applications.

Power electronic converters play a crucial role in the control and operation of modern pump systems. They provide a means to control the speed and torque of the motor, improve efficiency, and reduce energy consumption. Various types of converters can be used for pump applications, such as inverters, rectifiers, and cycloconverters. Each converter has its advantages and disadvantages, and the selection of the appropriate converter depends on the specific application requirements.

In recent years, there has been significant research on the design and development of power electronic converters for pump applications. The focus of these studies is to improve the efficiency and performance of the pump system, reduce energy consumption, and increase the reliability of the pump motor. This literature review aims to provide an overview of the different types of converters used for pump applications, their advantages and disadvantages, attained outcomes, research gaps, and references as illustrated in below Table 1.

C. RESEARCH GAPS

There are some potential research gaps related to converters for pump applications based on the literature review.

- Limited research on the use of power electronic converters in small-scale and rural water pumping systems, where access to reliable electricity is limited.
- Lack of studies on the integration of renewable energy sources with pump systems, and the use of power electronic converters to manage the energy flow.
- Limited research on the use of advanced control techniques, such as predictive control, model predictive control, and artificial intelligence-based control, to improve the performance and energy efficiency of pump systems with converters.
- Lack of studies on the impact of water quality and type on the performance and reliability of pump systems with converters.
- Limited research on the use of advanced materials and cooling techniques to improve the thermal management and reliability of power electronic converters in pump systems.

Addressing these research gaps can help improve the efficiency, reliability, and sustainability of pump systems with converters, and can enable the development of innovative and cost-effective solutions for water pumping in various applications. More specifically, from the study of the literature, speed regulation and fast response are the key factors for asynchronous motors. Hence, the design of the converter with a high step-up conversion ratio and better time response is essential. The overview of this complete literature does not deal with PV-QBC-GZSI-AMD. This research suggests a combination of QBC & GZSI to control AMD because the above literature did not report the speed regulation of PV-QBC-GZSI-AMD using a CM-HC controller since there is a need for constant speed AMD. Hence this work proposes CM-HC to control QBC-GZSI-AMD. This paper focuses on the identification of a controller for PV- QBC-GZSI-AMD that has high gain, a wide range of operations, and quick response.

The remaining sections of the article are organized as follows: Section II provides an in-depth explanation of the design and formulation of the proposed methodology. Section III presents the simulated results obtained from implementing the proposed methodology. In Section IV, the

TABLE 1. Literature survey and its inferences.

Converter	Advantages	Disadvantages	Attained Outcomes	Research Gaps	References
Three-Phase Z-Source Inverter	Boost feature, low cost, simple control	High THD, low efficiency	Achieved efficiency of 91%, boost feature	Analysis of dynamic performance needed	[10]
Five-Level Inverter	Improved quality of the output voltage waveform	Higher complexity and cost compared to traditional two-level inverters	Achieved efficiency of 95%, low THD, reduced size	Access to reliable electricity is limited	[11]
Nine-Switch Inverter	Higher number of switching states for increased flexibility and efficiency reduced harmonic distortion, and the ability to operate in standalone or grid-connected mode	High cost, complex topology	Achieved efficiency of 94%, reduced size, simple control	Limited analysis of dynamic performance	[12]
Direct Torque Control	High efficiency, simple control	High THD, limited operating range	Achieved efficiency of 90%, reduced size, simple control	Lack of studies on the integration of renewable energy sources	[13]
Three-Level T-Type Inverter	Low THD, high efficiency, reduced size, simple control	High cost, complexity in implementation	Achieved efficiency of 97%, low THD, reduced size	Limited analysis of dynamic performance	[14]
Single-Phase T-Type Inverter	Reduced number of switches, lower cost and complexity, and lower electromagnetic interference	Lower efficiency, higher harmonic distortion, and limited power handling capacity.	Achieved efficiency of 98%, low THD, reduced size	Limited analysis of dynamic performance	[15]
Three-Phase Dual Active Bridge Inverter	High efficiency, wide operating range, reduced size	Complex control, high cost	Achieved efficiency of 97%, low THD, reduced size	Lack of thermal management and reliability of power electronic converters in pump systems	[16]
Single-Phase Dual Active Bridge Inverter	High efficiency, low switching losses, and better power quality.	More complex control circuitry and higher cost compared to traditional inverters.	Achieved efficiency of 96%, low THD, reduced size	Limited analysis of dynamic performance	[17]
Single-Phase Quasi-Z-Source Inverter	High efficiency, low cost, simple control	Limited operating range, high THD	Achieved maximum efficiency of 95%, low THD	Limited analysis of dynamic performance	[18]
Single-Phase Zeta Inverter	Reduced component count and cost due to a simpler topology.	Limited range of output voltage due to the unidirectional nature of the inverter.	Achieved maximum efficiency of 92%, low THD	Limited analysis of dynamic performance	[19,20]

TABLE 1. *(Continued.)* **Literature survey and its inferences.**

Single-Phase Current Source Inverter with Voltage Booster	High output voltage gain, simpler circuit topology.	Complex control, high cost	Achieved maximum efficiency of 97%, low THD	Limited analysis of EMI	[21]
Three-Phase Inverter with Voltage Boosting Techniques	High efficiency, wide operating range	Lower efficiency, and higher cost	Achieved maximum efficiency of 97%, low THD	Limited analysis of EMI	[22]
Single-Phase Transformerless Inverter with Modified SVPWM	High efficiency, low cost, simple control	Limited operating range	Achieved maximum efficiency of 92%, low THD	No analysis of dynamic performance	[23]
Dual-Boost Single-Phase High-Frequency Link Converter	Wide operating range, high efficiency	Complex control, high cost	Achieved maximum efficiency of 98%, low THD	Limited analysis of EMI	[24]
Single-Phase High-Efficiency Inverter	High efficiency, low cost, simple control	Limited operating range, high THD	Achieved maximum efficiency of 91%, low THD	Limited analysis of pump load characteristics	[25]
Capacitor-Coupled Boost Converter-Based Pumping Inverter	High efficiency, wide input voltage range	Complex control, high cost	Achieved maximum efficiency of 98%, low THD	Limited analysis of dynamic performance	[26]
Extended Coupled-Inductor QZS Inverter	Reduction of input current ripple	High cost, complex topology	Achieved efficiency of 96%, low THD, reduced size	Limited analysis of dynamic performance	[27]

hardware design is discussed, along with its corresponding outcomes. Section V presents a comparative study between the achieved outcomes of the proposed method and existing topologies. Finally, Section VI concludes the work based on the attained outcomes from the entire study.

II. DESIGN AND FORMULATION OF THE PROPOSED METHODOLOGY

A. QUADRATIC-BOOST CONVERTER (QBC)

QBC is a power electronic converter that allows bidirectional power flow with a single switch [28]. They have attracted significant attention in recent years due to their potential applications in energy storage systems, electric vehicles, and renewable energy systems. QBCs can operate in both buck and boost modes, and they provide high efficiency, low harmonic distortion, and fast dynamic response. However, the design and control of QBCs can be challenging due to their complex and nonlinear behavior. Therefore, accurate and reliable modeling of QBCs is crucial for their optimal design and control. In this context, various modeling approaches have been proposed, ranging from simple analytical models to complex simulation-based models, considering different levels of abstraction and accuracy. The selection of the modeling approach depends on the application and the required level of detail. A quadratic boost converter is a DC-DC boost converter with a second phase that boosts DC voltage. The output voltage of a quadratic boost converter is always greater than the input voltage. The following equations can be used to compute the output voltage:

$$V_{OUT} = \frac{V_{IN}}{(1-D)^2} \tag{1}$$

Specifically, MOSFETs (Q) serve as switches, while inductors (L), diodes (D), capacitors (C), and resistors (R) serve as loads in the Quadratic Boost Converter circuit depicted in Figure 1.

The circuit will operate based on the assumption. If the switch (Q) is in ideal the capacitors C1 & C2 are assumed to be large and the voltage on the capacitors VC1 and VC2 is approximately stable throughout the switching process. Equation (2) is used to calculate the gate current in the

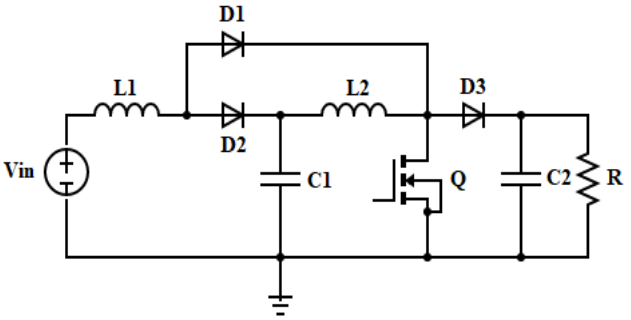

FIGURE 1. Quadratic boost converter circuit.

MOSFET, where P_G is the power at the gate, V_G is the voltage at the input multiplied by the duty cycle % (D).

$$I_G = \frac{P_G}{V_G} \tag{2}$$

$$P_G = F_S Q_G V_G;\ V_G = V_G D \tag{3}$$

$$L = \frac{(1-D)^2 DR}{2Fs} \tag{4}$$

$$C_1 = \frac{IoD}{(1-D)\,\Delta Vc1Fs} \tag{5}$$

$$C_2 = \frac{IoD}{\Delta Vc2fs} \tag{6}$$

where, I_G = Current at the gate terminal; V_G = Voltage at the gate terminal; P_G = Power at the gate terminal; F_S = Switching frequency; L= Inductance; R= Resistance; Io = Output current.

B. ANALYSIS OF QBC-GZSI

QBC-fed Gamma Z-Source Inverters (GZSI) are the popular power converters used in renewable energy and electric vehicle applications. GZSI provides a unique buck-boost capability, which allows for the regulation of the output voltage even when the input voltage is lower than the output voltage. This topology has several advantages over traditional inverters, such as a reduced number of components, lower electromagnetic interference, and improved efficiency. However, the design and control of QBC-fed GZSI can be challenging due to their complex nonlinear behavior. Therefore, mathematical modeling of QBC-fed GZSI is crucial for the optimization of their design and control strategies. Different modeling techniques have been proposed for QBC-fed GZSI, ranging from analytical models to simulation-based models, considering different levels of complexity and accuracy. The selection of the modeling technique depends on the specific application and the desired level of detail. The first two out of seven operating stages of PV-QBC-GZSI are explained here.

Stage I: Charging circuit (Figure 2)

The relevant voltage equations are as follows:

$$V_{C1} + V_{L2} = 0 \tag{7}$$

$$Vin = V_{L1} + V_{C1} \tag{8}$$

$$Van = V_G/2 \tag{9}$$

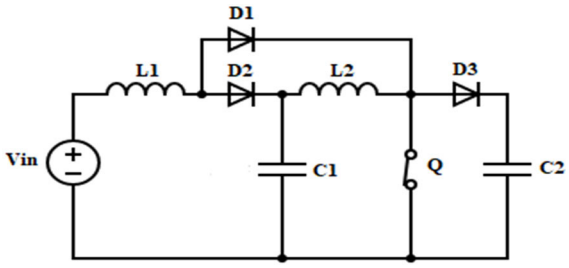

FIGURE 2. Stage-I: charging circuit.

$$Vbn = -V_G/2 \tag{10}$$

Stage II: Discharging circuit (Figure 3)

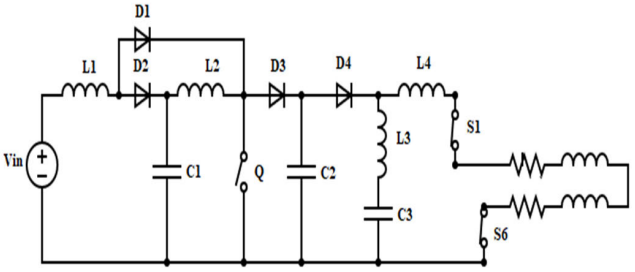

FIGURE 3. Stage-II - S1 and S6 ON.

The relevant voltage equations are as follows:

$$V_{in} = V_{L1} + V_{C1} \tag{11}$$

$$V_{C1} + V_{L2} = V_{C2} \tag{12}$$

$$Van = V_G/2 \tag{13}$$

$$Vbn = -V_G/2 \tag{14}$$

Further, the stages III to VII are similar to stage II with switching sequences of 12, 23, 34, 45, and 56.

C. BLOCK DIAGRAM OF THE PROPOSED METHOD

The block diagram of PV-QBC-GZSI-AMD is shown in Figure 4. The output of PV is used to charge the battery and the constant voltage from the battery is stepped up using QBC. Also, the output of QBC is inverted and applied to 5HP-IM. The control unit of GZSI-AM is used to apply pulses to QBC & GZSI and the block structure of closed-loop PV-QBC-GZSI-AMD using CM-FOPI, CM-PR, and CM-HC controller is delineated in Figure 4. PI-controlled AMD has disadvantages like high overshoot, sensitivity to controller gain, and sluggish response. On the other hand, PID-controlled AMD has drawbacks like instability due to input signals and sensitivity to noise errors. Hence, this work has considered controllers like CM-FOPI, CM-PR and CM-HC. The speed of the Asynchronous motor is sensed then it is compared with the reference speed to obtain Speed Error (SE). The SE acts as a virtual current reference and it is applied to speed FOPI/PR/HC-1. Moreover, the specifications of the Asynchronous motor are given in Table 2.

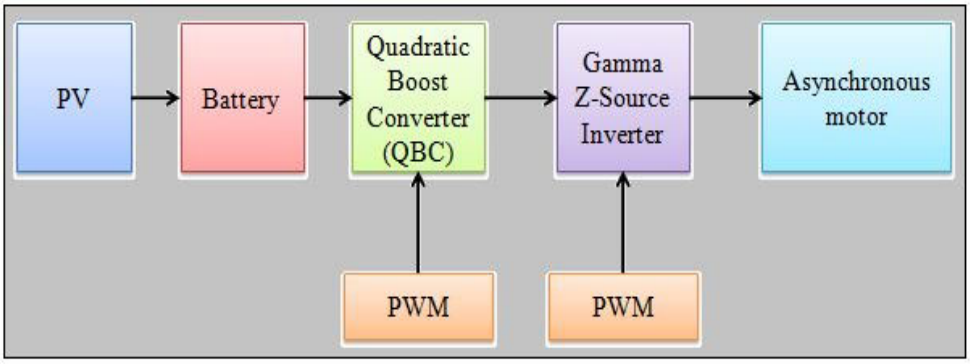

FIGURE 4. Lock diagram of the model based on PWM.

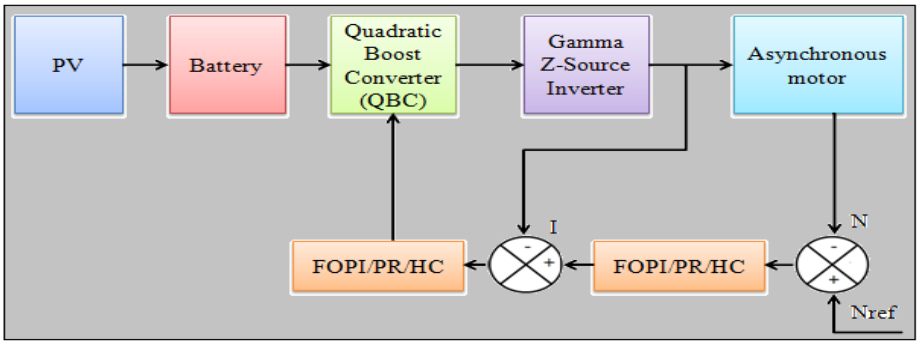

FIGURE 5. Block diagram of proposed PV-QBC-GZSI-AMD.

The output of FOPI/PR/HC-1 is compared with the actual current and error is applied to FOPI/PR/HC-2. The output of controller-2 updates the duty cycle of the QBC. Figure 5 illustrates the block diagram of closed-loop PV-QBC-GZSI-AMD using CM-FOPI, CM-PR, and CM-HC controllers.

Hysteresis Controller:

Hysteresis controller is also called Bang-Bang controller and its frequency is kept constant with varied pulse width. When the difference between the reference and actual value crosses the positive and negative band, pulses are inhibited. This controller provides inherent over-current protection and the hysteresis band is defined as follows:

$$I_B = I_U - I_L \tag{15}$$

where

I_U - Upper limit of current

I_L – Lower limit of current

Also, the hysteresis controller does not require detailed analysis and its output is free from chattering.

Design Considerations:

The following assumptions were made to design QBC-GZSI-AMD.

Fs = 5 kHz, Vi = 48V, Vo = 400 V $\Delta Vc_2 = 0.1$ R=2.5Ω

$$V_{OUT} = \frac{V_{IN}}{(1-D)^2}, \text{D works out to } 0.65 \tag{16}$$

T_{ON} works out to 0.13ms and T_{OFF} works out to 0.07ms

$$L = \frac{(1-D)^2 DR}{2fs}; L \text{ works out to } 0.02 \text{ mH} \tag{17}$$

$$C_1 = \frac{IoD}{(1-D)\,\Delta Vc1fs}; C_1 \text{ works out to } 1\ \mu F \tag{18}$$

$$C_2 = \frac{IoD}{\Delta Vc2\ fs}; C_2 \text{ works out to } 9000\ \mu F \tag{19}$$

TABLE 2. Specifications of asynchronous motor.

Parameter	Value
Voltage (Line-Line)	60 Vrms
Frequency	50 Hz
Stator Resistance	1.15Ω
Stator Inductance	0.005974H
Rotor Resistance	1.83Ω
Rotor Inductance	0.005974H
Mutual Inductance	0.2037H
Inertia	0.02 Kg/m^2
Friction Factor	0.005752 N-m
Pole pairs	2

D. EVALUATION ALGORITHM

The methodology to evaluate the performance of the proposed methodology is shown in Figure 6. The research

TABLE 3. Simulation parameters of PV-QBC-GZSI-AMD.

Parameter	Value
Vin	48V
C1	1μF
L1,L2	0.02mH
C2	9000μF
C3	2000μF
L3	0.9μH
L4	0.009 μH
Switching Frequency	5kHz
Pulse width	65%
MOSFET(IRF840)	500V/8A
Motor	440V/5HP/1440rpm

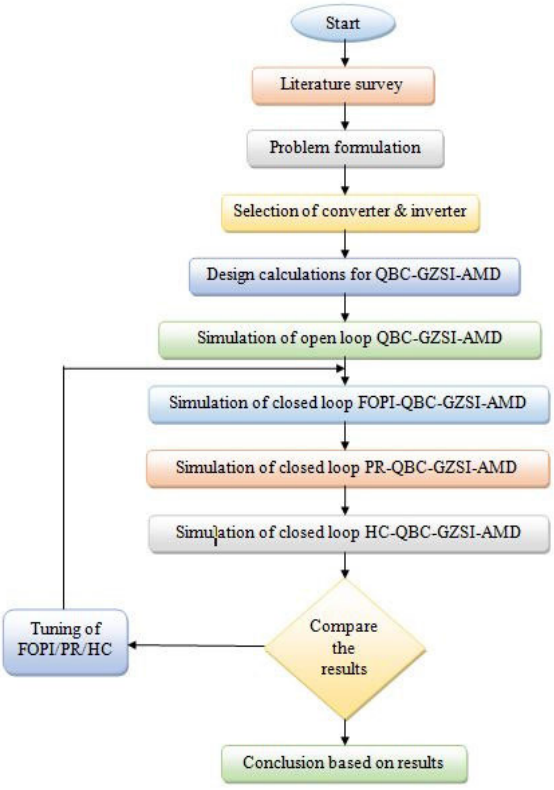

FIGURE 6. Methodology flow chart for QBC-GZSI-AMD.

problem is formulated based on a literature survey on AMD. After selecting the converter and inverter, design calculations are made. Simulation of closed-loop PV-QBC-GZSI-AMD with FOPI, PR, and HC are performed to identify better controllers in the closed loop.

III. SIMULATION RESULTS

The PV-QBC-GZSI-AMD is operated in the current control mode. Then PI controllers are replaced with FOPI, PR, and HC controllers, and the speed and torque are measured. Here the dynamic performance of the controllers is compared. The reference speed is evaluated with the actual speed to provide the error signal. The obtained signal is related to the current to get the PWM signal for QBC. This error signal is coursed by the FOPI, PR, and HC to sustain the constant speed and diminish the steady-state errors. The main ease of these control methods is easy control and good speed regulation. Closed loop simulation of PV-QBC-GZSI-AMD is done with FOPI, PR, and HC controllers and the results are analyzed here. Table 3 outlines the simulation parameters of PV-QBC-GZSI-AMD.

A. CLOSED LOOP CM-FOPI CONTROL PV BASED QBC FED GZSI WITH ASYNCHRONOUS MOTOR

The circuit diagram of Closed-loop- CM-FOPI control PV-QBC-GZSI-AMD is delineated in Figure 7. Scopes are connected to display the output voltage of QBC and GZSI. Scopes connected to AMD indicate the speed, torque, and mechanical power of AMDS. Speed signal is sensed then it is compared with ref-speed. The SE is given to FOPI-1. The output of FOPI-1 is compared with the current signal and CE is applied to FOPI-2. The output of FOPI-2 is used to update the duty ratio of MOSFET in QBC. The input voltage of closed-loop- CM-FOPI control PV-QBC-GZSI-AMD is represented in Figure 8 and its value increases from 50V to 70V due to positive step change in input voltage.

B. CLOSED LOOP CM-PR CONTROL PV BASED QBC FED GZSI WITH ASYNCHRONOUS MOTOR

The time response of PV-QBC-GZSI-AMD with CM-FOPI is sluggish. Hence it is proposed to control PV-QBC-GZSI-AMD using a CM-PR controller. The Circuit diagram of closed-loop-CM-PR control PV-QBC-GZSI-AMD is delineated in Figure 9. Scopes are connected to the output of the inverter to measure line-to-line voltages. The actual speed of AMD is compared with the set speed and speed error is obtained. The SE represents virtual set current (VSC) and it is compared with actual current and current error is applied to PR-2. Then, the output of PR-2 is applied to the Pulse Generation Block (PGB) which updates the Pulse width of QBC.

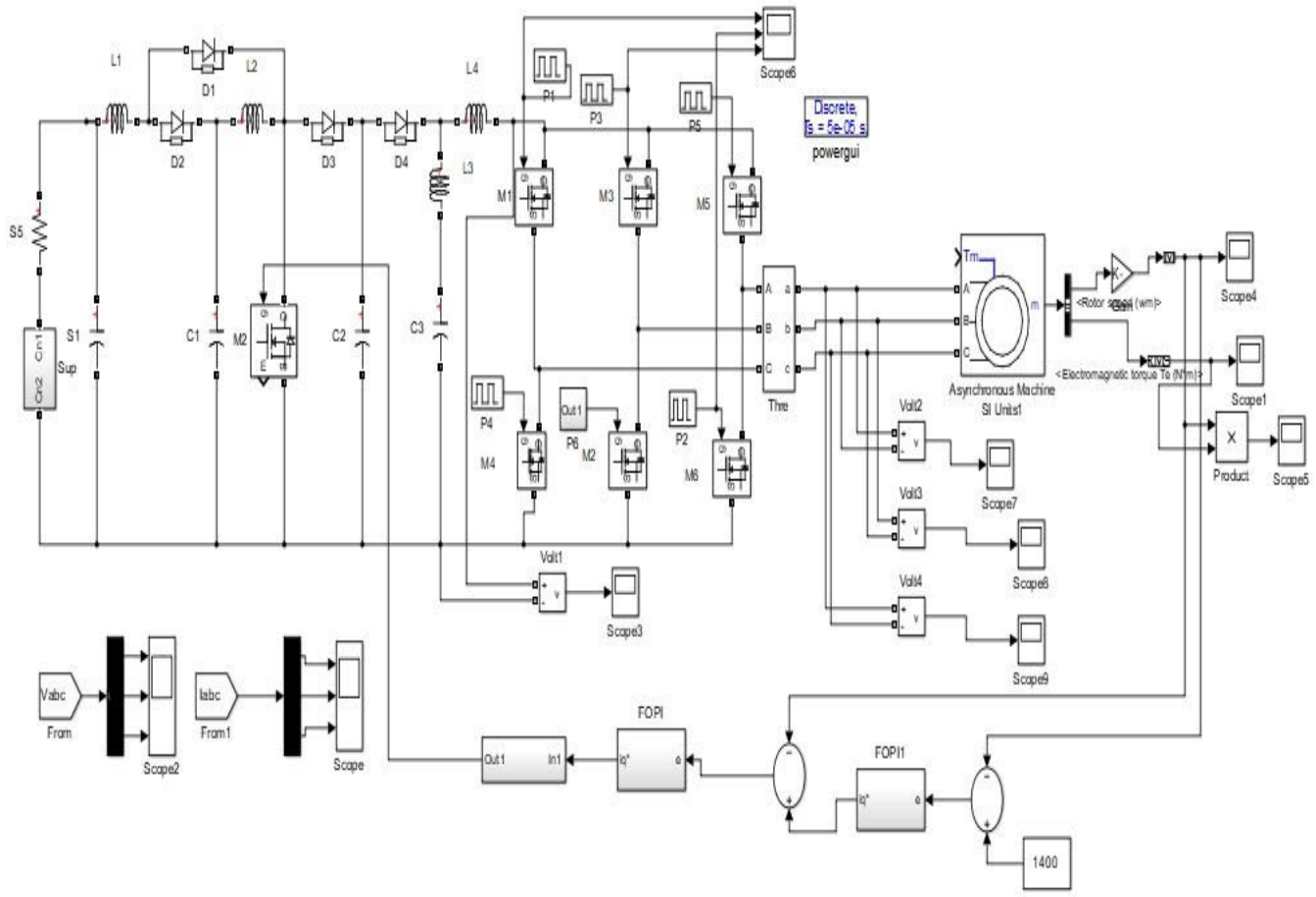

FIGURE 7. Simulation of CM-FOPI controlled PV-QBC-GZSI-AMD in MATLAB/simulink.

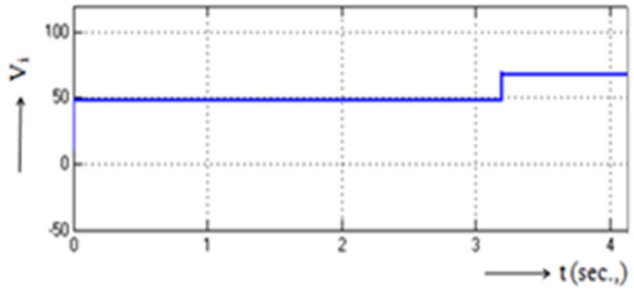

FIGURE 8. Input voltage of CM-FOPI controlled PV-based QBC fed GZSI with AMD.

C. CLOSED LOOP CM-HC CONTROL PV BASED QBC FED GZSI WITH ASYNCHRONOUS MOTOR

The time response of PV-QBC-GZSI-AMD with CM-FOPI and CM-PR is sluggish. Hence, it is proposed to control PV-QBC-GZSI-AMD using a CM-HC controller. The Circuit diagram of closed-loop-CM-HC control PV-QBC-GZSI-AMD is delineated in Figure 10. Scopes connected to the gates of switches indicate switching pulses. The rotor speed of AMD is compared with set speed and the SE is applied to PI-1 controller. The output of PI-1 acts as a current reference and it is compared with the actual current to produce current error. The CE is applied to HC. The output of HC is used to adjust the duty ratio of QBC.

Figure 11 illustrates the motor speed in the closed-loop PV-QBC-GZSI-AMD system, employing CM-FOPI, CM-PR, and CM-HC control strategies. Specifically, the motor speed is measured at 1407 RPM with CM-FOPI, 1381 RPM with CM-PR, and 1365 RPM with CM-HC. To provide a more detailed view of the motor speed control with CM-FOPI, CM-PR, and CM-HC in the PV-QBC-GZSI-AMD setup, Figure 12 presents a zoomed-out perspective. Furthermore, Figure 13 portrays the torque response in the closed-loop CM-FOPI, CM-PR, and CM-HC control of the PV-QBC-GZSI-AMD system. The torque values for the motor are 3.9 N-m with CM-FOPI, 3.6 N-m with CM-PR, and 1.9 N-m with HC. It is noteworthy that the torque developed is at its minimum when using the HC control strategy.

The motor speed with CM-HC is found to be slightly less than that of CM-FOPI and CM-PR-controlled PV-QBC-GZSI-AMD. The torque with CM-FOPI is higher than that of CM-PR and CM-HC-controlled PV-QBC-GZSI-AMD. The time response method is used to study the performance of closed-loop PV-QBC-GZSI-AMDS.

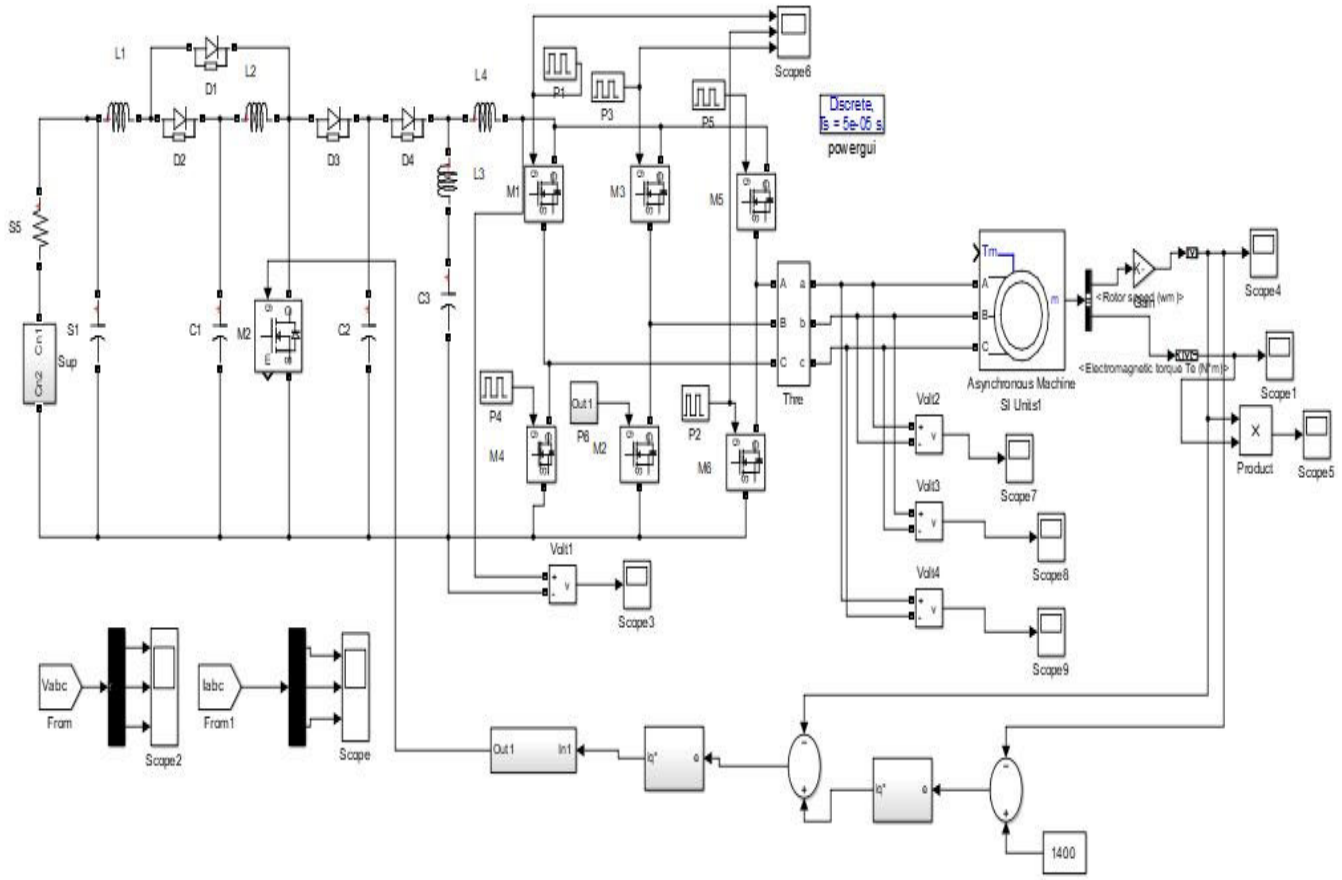

FIGURE 9. Simulation of CM-PR controlled PV-QBC-GZSI-AMD in MATLAB/simulink.

The performance of closed-loop PV-QBC-GZSI-AMDS with various controllers is compared using time domain parameters.

D. COMPARISON OF TIME DOMAIN PARAMETERS

Figure 14 (a) outlines the time domain parameters for a speed of 1300 RPM using CM-FOPI, CM-PR, and CM-HC controller. While using the CM-HC controller, the rise dwindled from 3.28 Sec to 3.26 Sec; the Peak dwindled from 3.40 Sec to 3.29 Sec; Settling-time dwindles from 3.63 Sec to 3.45 Sec; Steady-state-error dwindled from 3.80 RPM to 2.15 RPM. Similarly, the test is carried out for different motor speeds and illustrated in the below Figures.

Further, the time domain parameters for torque with a ref speed of 1300 RPM using CM-FOPI, CM-PR, and CM-HC controller are illustrated in Figure 15 (a). By using the CM-HC controller, rise time dwindles from 3.38 Sec to 3.35 Sec; peak time dwindles from 3.45 Sec to 3.36 Sec; settling dwindles from 3.92 Sec to 3.61 Sec; steady-state-error is dwindled from 0.82 to 0.46 N-m.

The above figure outlines the time response with a change in input voltage/change in load. With a 20% increase in input voltage, the Steady-state dwindled from 3.62 RPM to 1.97 RPM; the settling time dwindled from 3.58 Sec to 3.42 Sec. With a 20% decrease in input voltage, the Steady-state dwindled from 3.66 RPM to 1.98 RPM; the settling time dwindled from 3.59 Sec to 3.43 Sec. With a 10% increase in input voltage, the steady-state error dwindles from 3.60 RPM to 1.98 RPM and Settling-time is dwindled from 3.55 Sec to 3.39 Sec. With a 10% decrease in input voltage, the Steady-state dwindles from 3.61 RPM to 1.99 RPM; the settling time dwindles from 3.56 Sec to 3.40 Sec. With a 10% decrease in load, the Steady-state-error dwindles from 3.67 RPM to 2.01 RPM and Settling-time is dwindled from 3.58 Sec to 3.45 Sec. In Nutshell, by using CM-HC (Motor speed), Rise-time, Peak-time, and Steady-state-error are reduced. Also, by using CM-HC (Motor torque), Rise-time, Peak-time, and Steady-state-error are reduced. Hence, the outcome illustrates that the closed-loop PV-QBC-GZSI-AMD with CM-HC is superior to closed-loop PV-QBC-GZSI-AMD with CM-FOPI and CM-PR controllers.

IV. HARDWARE RESULTS

Figure 16 depicts the proposed hardware configuration for the pump application converter. This setup comprises a PV panel, a rectifier unit, a QBC-GZSI module, a control block, an inverter, and an asynchronous motor. To regulate the duty cycles of both QBC and GZSI, the project employs a

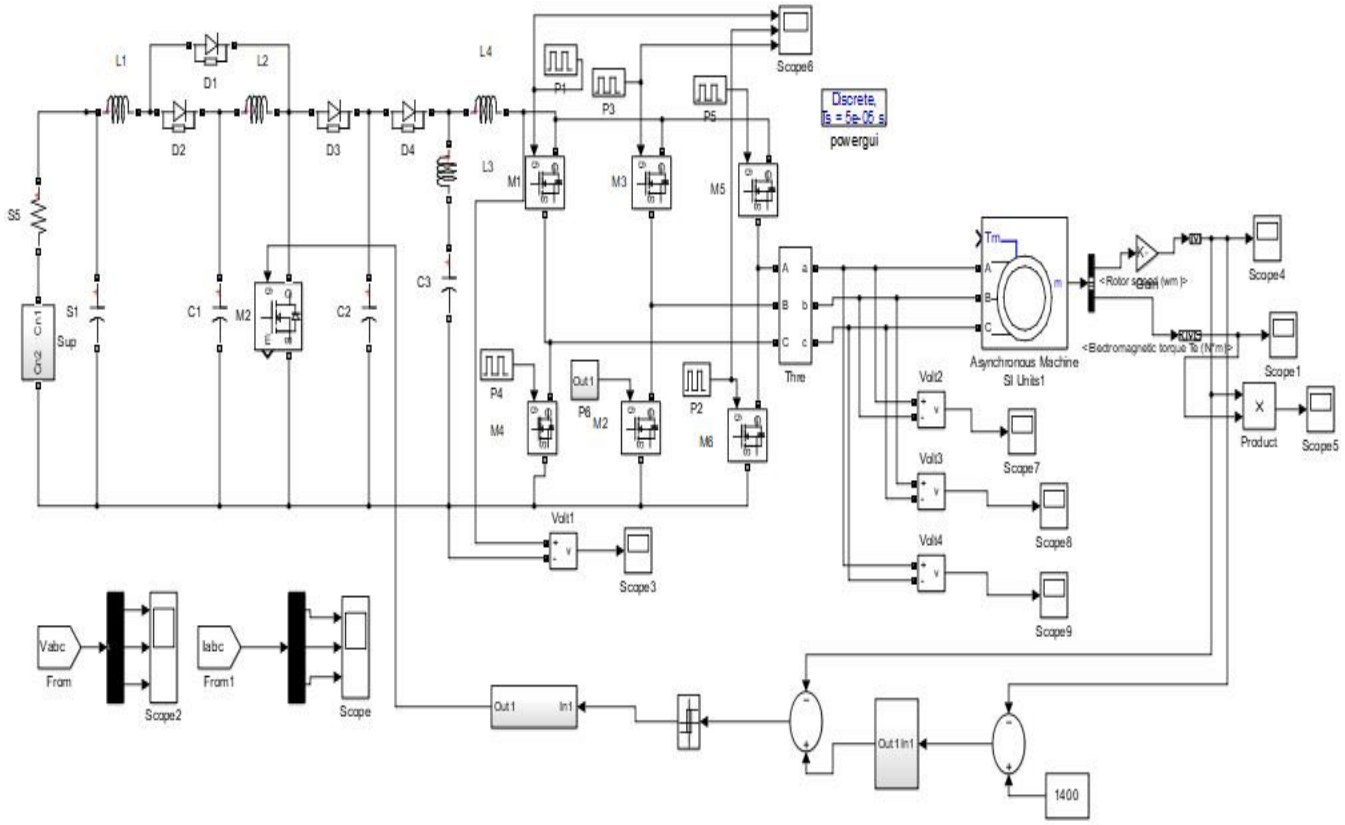

FIGURE 10. Simulation of CM-HC controlled PV-QBC-GZSI-AMD in MATLAB/simulink.

TABLE 4. Time response with change in input voltage/change in load.

System Response	Specifications	FOPI	PR	HC
20% increase in input	Steady-state error	3.62	2.68	1.97
	Settling time(sec)	3.58	3.49	3.42
20% decrease in input	Steady-state error	3.66	2.69	1.98
	Settling time(sec)	3.59	3.50	3.43
10% increase in input	Steady-state error	3.60	2.65	1.98
	Settling time(sec)	3.55	3.46	3.39
10% decrease in input	Steady-state error	3.61	2.66	1.99
	Settling time(sec)	3.56	3.47	3.40
10% decrease in load	Steady-state error	3.67	2.69	2.01
	Settling time(sec)	3.58	2.67	3.45

PIC16F84, which generates pulses subsequently amplified by an IR2110 driver board. The control circuit within the PV-QBC-GZSI-AMD system is outlined in Figure 17. Port-A is dedicated to reading the actual speed, while port-B is utilized for pulse output to QBC and GZSIC. Speed and current errors are computed through specialized algorithms based on speed and current measurements.

The hardware results offer valuable insights into the system's time response characteristics under varying input voltage and load conditions. The analysis focuses on key parameters such as steady-state error and settling time, which were assessed across different system behaviors, including scenarios involving a 20% increase and decrease in input voltage, as well as a 10% variation in both input and load. Notably, the HC control strategy consistently demonstrated exceptional performance. For instance, during a 20% increase in input voltage, it achieved an impressively low steady-state error of 1.97 RPM and a rapid settling time of 3.42 seconds. Similarly, for other tested scenarios, such as input voltage reduction and load decrease, the HC control strategy consistently delivered minimal steady-state error and swift settling times, highlighting its effectiveness in maintaining

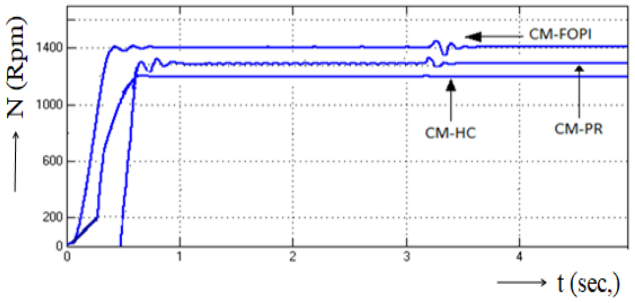

FIGURE 11. Motor speed of CM-FOPI, CM-PR, and CM-HC control PV-QBC-GZSI-AMD.

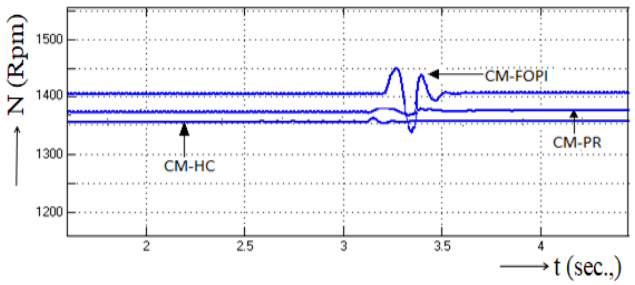

FIGURE 12. Motor speed Zoom out of CM- FOPI, CM-PR, and CM-HC control PV-QBC-GZSI-AMD.

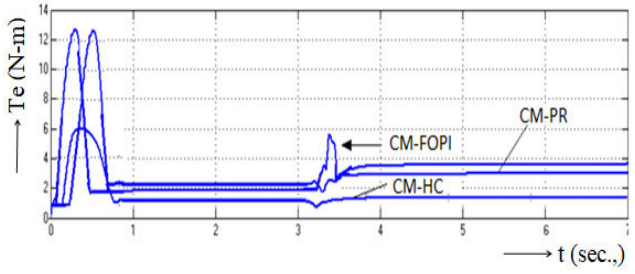

FIGURE 13. Motor Torque of CM-FOPI, CM-PR, and CM-HC control PV-QBC-GZSI-AMD.

system stability and precision within the PV-QBC-GZSI-AMD setup.

Additionally, Figure 18 provides a visual representation of the Digital Storage Oscilloscope (DSO) output, showcasing the DC input voltage supplied to the QBC (Quantum Boost Converter). It's worth noting that the output voltage of the QBC exhibits minimal ripple, underscoring the converter's stability and efficient operation in maintaining a steady output voltage. Figure 19 shows the DSO output of the DC Input current to QBC observed as 63.6A. Further, Figure 20 shows the DSO output of Voltage across QBC. Moreover, Figure 21 delineates the DSO output of Switching-Pulse for inverters M1, and M3 followed by Figure 22 which shows the DSO output of Switching Pulse for inverters M2, and M4. Then, Figure 23 illustrates the DSO output of Voltage across the motor load, and Figure 24 represents the DSO output of current through the motor load. Based on the observed figures, the distortion in the current through AMD is observed due to a change in the switching sequence of GZSI for every 60-degree interval.

V. COMPARATIVE STUDY

Table 5 provides a comprehensive overview of the comparison between simulation and experimental results in the context of the proposed converter. Notably, the alignment between simulated and experimental values is discussed for various parameters, shedding light on the performance of the system. One key observation from the comparison is the close agreement between simulated and experimental values for critical parameters such as DC input voltage and gate-to-source voltage. This alignment indicates that the simulation model accurately represents the real-world behavior of the proposed converter under specific operating conditions.

Furthermore, the comparison extends to the DC output voltage and AC output voltage, revealing a remarkable similarity between the two sets of results. However, a slight reduction is noted in the experimental values for the PV-QBC-GZSIS configuration. For instance, the simulation reports a DC output voltage of 400 V, whereas the hardware measurement yields a slightly lower value of 391 V. Similarly, the AC output voltage in the simulation stands at 400 V, while the experimental result registers a slightly reduced value of 385 V. To understand the source of these discrepancies, a detailed analysis is conducted, attributing the variations to voltage drops occurring in various components. Components such as devices, chokes, and the equivalent series resistance (ESR) of capacitors within the QBC and GZSIC contribute to these differences. This nuanced understanding of the factors influencing the results enhances the credibility of the comparison and underscores the complexities involved in translating simulation outcomes to real-world experimental setups.

The stator current is another parameter examined in the comparison, with the simulation recording a value of 7.4 A and the hardware measurement reporting a slightly lower value of 7.2 A. This discrepancy is attributed to the decrease in applied voltage in the hardware setup due to device drops. Understanding such nuances is crucial for refining the simulation model and improving its accuracy in predicting real-world behavior.

Efficiency is a key performance metric for any power converter, and the proposed converter is evaluated in this regard. The efficiency is computed between the input and output of the QBC-GZSI-AMD, resulting in values of 90.82% for the experimental setup and 96.65% for the simulation. This disparity prompts a closer examination of the factors influencing efficiency in both scenarios. The observed efficiency is then benchmarked against existing converters, providing valuable insights into the performance of the proposed converter concerning other topologies. Comparisons are made with converters such as the Differential Boost Inverter (DBI) with an efficiency of 83.4%, Quasi Z-Source Inverter (QZSI) at 90.2%, Switched-coupled inductor inverter (SCII) at 89.9%, Improved Differential Boost Inverter (IDBI) at 92.5%, and Quasi-Z-Source Boost DC-DC Converter (QZS-DC-DC) at

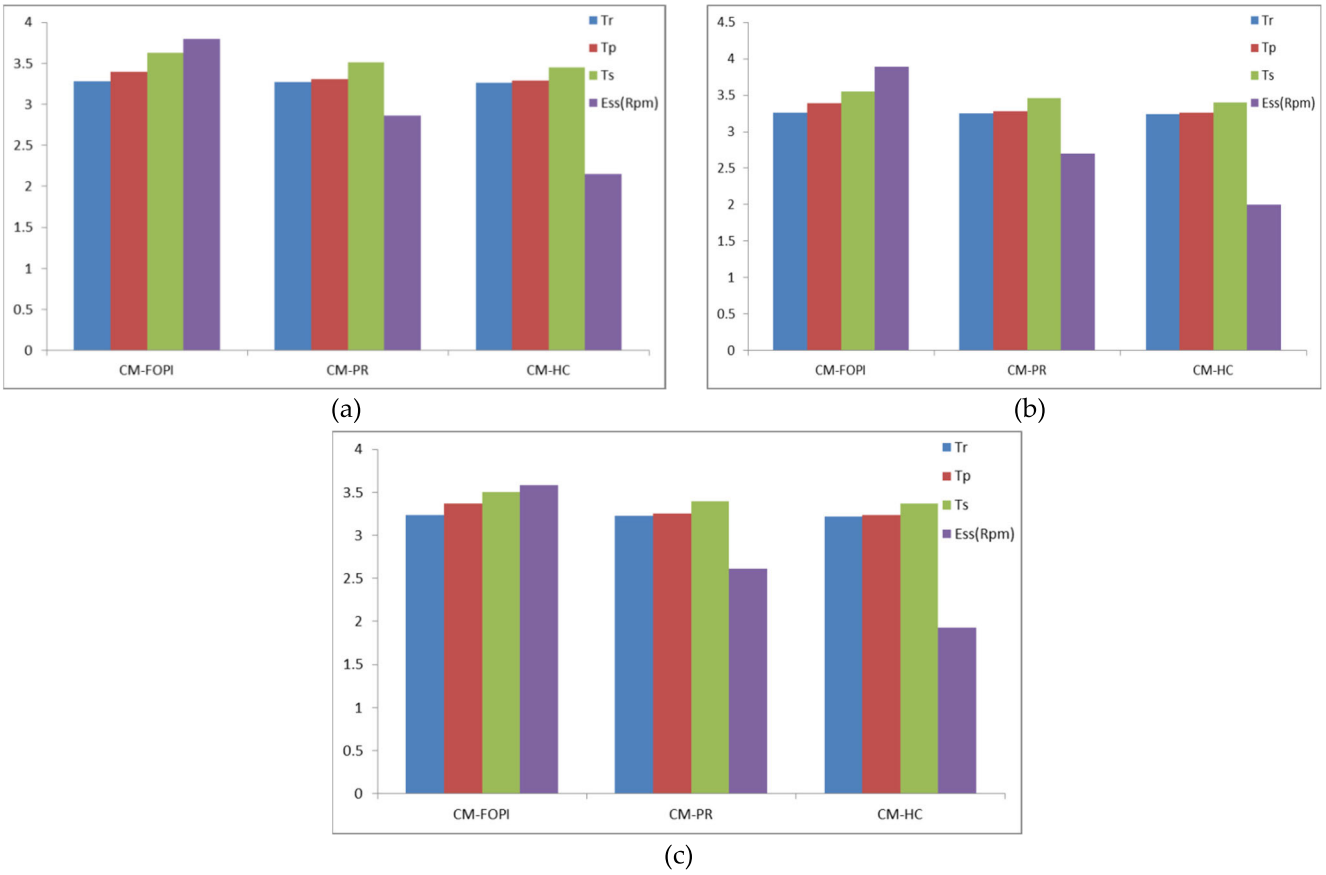

FIGURE 14. Comparison time domain parameters of motor speed (a) 1300 rpm (b) 1350 rpm and (c) 1400 rpm.

95.4%. The results of these comparisons highlight the competitive edge of the proposed converter, which attains a higher efficiency rate compared to other relevant converter topologies. This finding reinforces the significance of the proposed method and positions it favorably in the landscape of power converters.

TABLE 5. Simulation and experimental values.

Parameter	Simulation Value	Experimental Value
DC Input voltage	48 V	48 V
DC Input current	63.8 A	63.6A
Gate to Source voltage	10 V	10 V
DC Output voltage	400 V	391 V
AC Output voltage	400 V	385 V
Stator current	7.4 A	7.2 A

Additionally, the performance of the proposed converter topology is assessed by comparing it to notable existing works, considering key factors such as the number of stages, number of loops, control method, load type, performance parameters, and any associated drawbacks. A comprehensive summary of this comparative analysis is provided in Table 6. Notably, the proposed QBC-GZSIC configuration stands out for its efficiency, utilizing only two loops and proving to be particularly well-suited for high-power drive applications.

TABLE 6. Comparison of the proposed work.

Parameter	Existing Work [29]	Existing Work [30]	Proposed Work
No of stages	2	3	2
No of loops	Zero	2	2
Control method	Open loop control	Hysteresis controller	Hysteresis controller
Load	Three-phase induction motor	Single-phase induction motor	Three-phase induction motor
Performance parameters	NA	Time response	Time response
Advantage/Drawback	Poor regulation	Suitable for low-power drives	Suitable for high-power drives

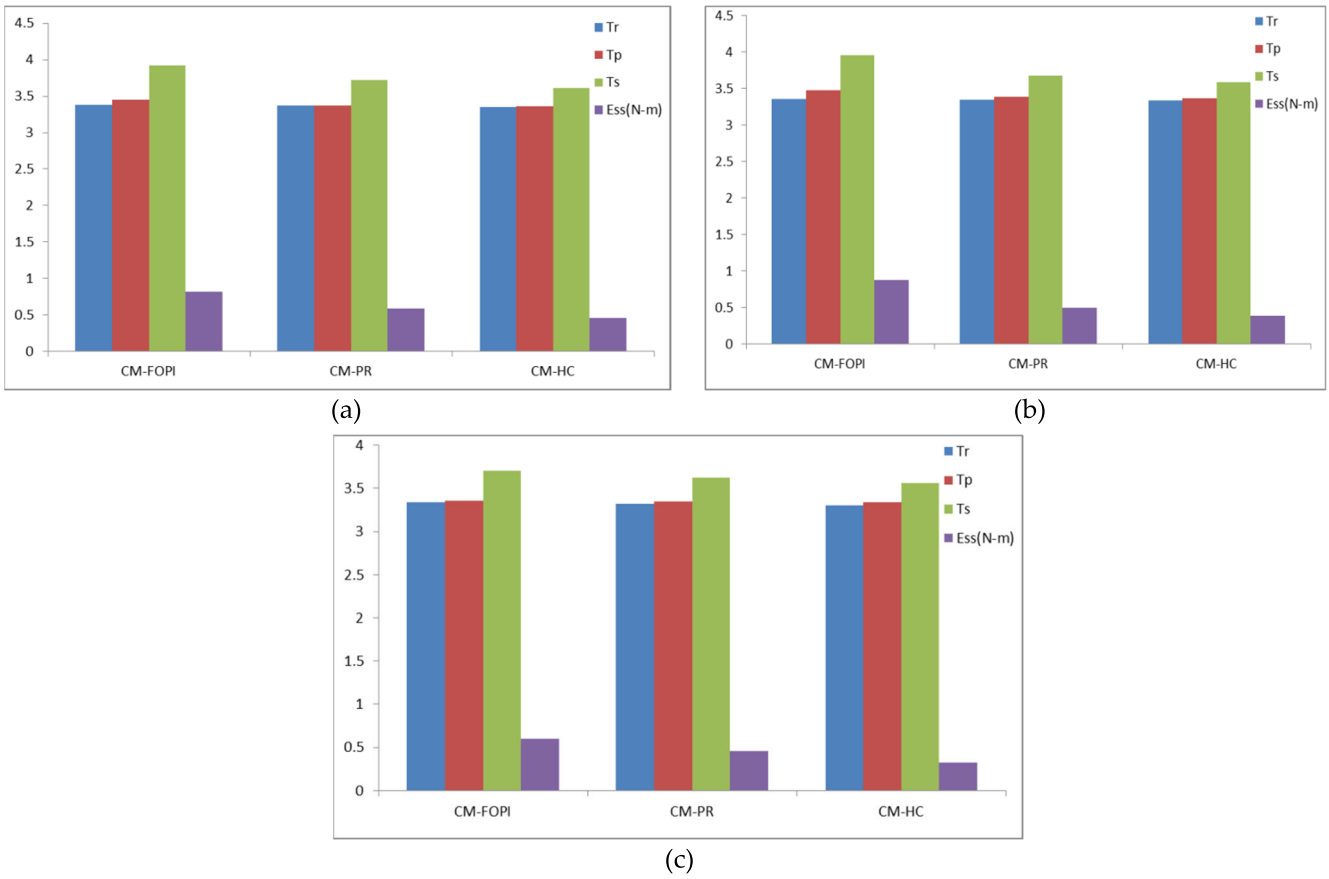

FIGURE 15. Comparison time domain parameters of motor torque (a) 1300 rpm (b) 1350 rpm and (c) 1400 rpm.

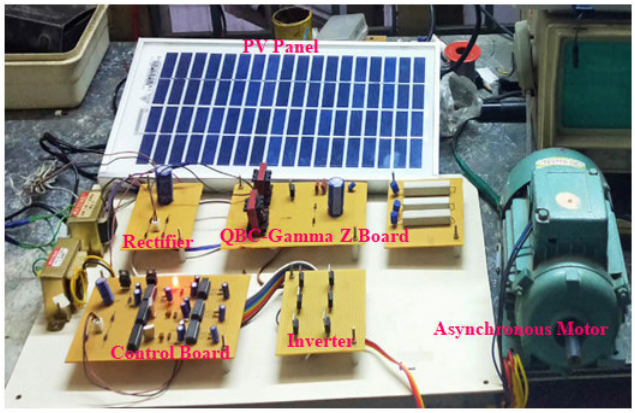

FIGURE 16. Hardware snapshot of PV-QBC-GZSI-AMD.

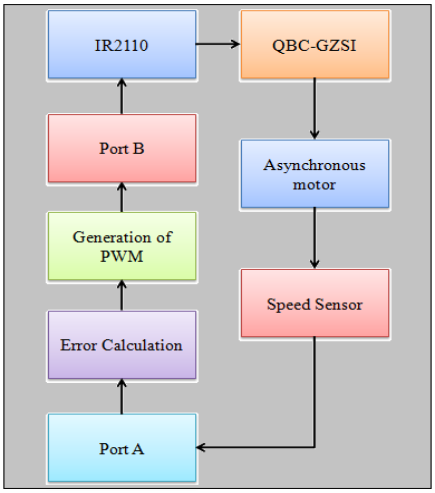

FIGURE 17. Control circuit employed in PV-QBC-GZSI-AMD.

It is found that the proposed PV-QBC-GZSIS converter model provided better results compared with other existing topologies and its reliability is tested and compared with experimental results. The combination of the three topologies has resulted in a high-performance and efficient pumping system. The use of the photovoltaic system ensures a clean and sustainable source of energy for powering the pumping system, while the QBC and Gamma Z source inverter help regulate and control the power supply to the motor. However, there is still room for further investigation and improvement of the photovoltaic-QBC-Gamma Z source

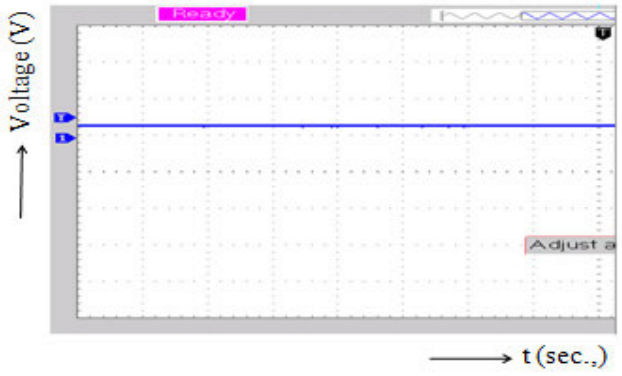

X-axis 1unit=0.2ms Time Y-axis 1div =40v.

FIGURE 18. DC Input voltage to QBC of PV-QBC-GZSI-AMD.

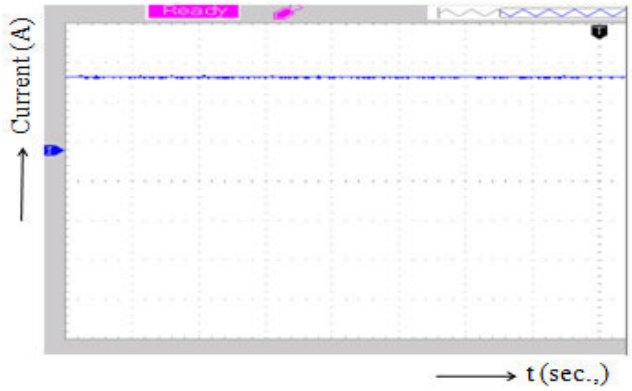

X-axis 1 unit =0.2ms Y-axis 1div = 25A

FIGURE 19. DC Input current to QBC of PV-QBC-GZSI-AMD.

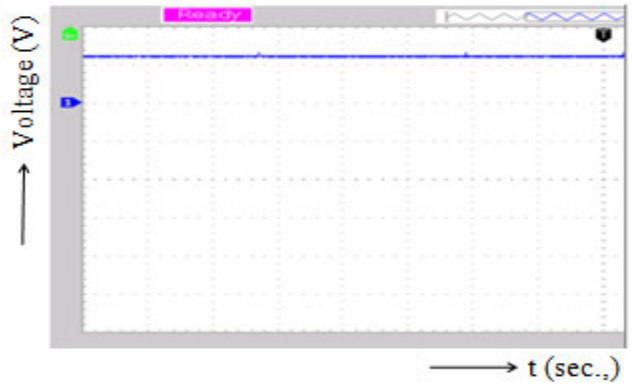

X-axis 1unit=0.2μs Time Y-axis 1div =100v

FIGURE 20. Voltage across QBC of PV-QBC-GZSI-AMD.

X-axis 1unit=0.2ms Time Y-axis 1div =2v

FIGURE 21. Switching Pulse for inverter M1, M3.

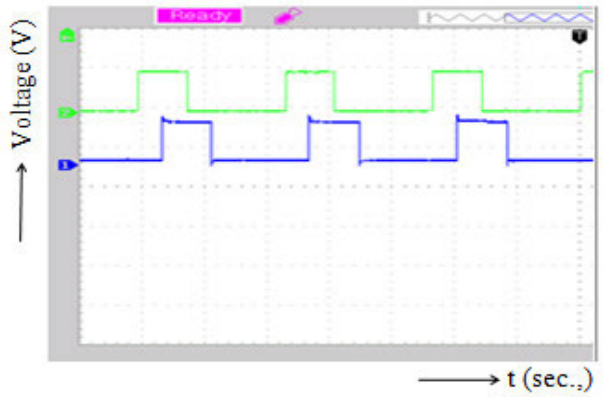

X-axis 1unit=0.2ms Time Y-axis 1div =2v

FIGURE 22. Switching Pulse for inverter M2, M4.

X-axis 1unit=0.2ms Time Y-axis 1div =100v

FIGURE 23. Voltage across a motor load of PV -QBC-GZSI-AMD.

inverter. One possible area of improvement is the development of advanced control strategies that can improve the system's efficiency and reliability. For instance, the use of model predictive control algorithms or Artificial Intelligence-based controllers can help optimize the system's performance and improve its energy efficiency. In a nutshell, the Photovoltaic-QBC-Gamma Z source inverter has proven to be an effective technology for pumping applications. However, further research is needed to improve the system's control strategies and power electronics devices, which can help optimize its performance and improve its energy efficiency.

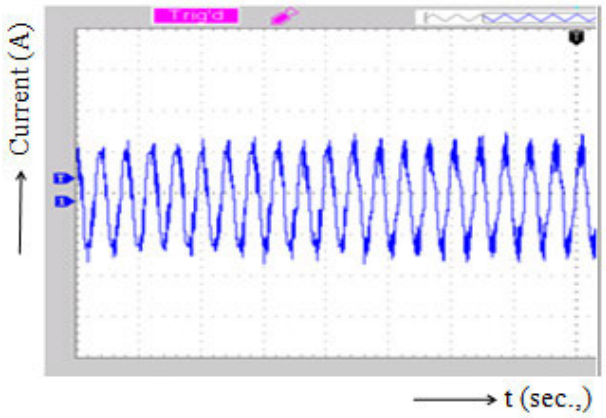

X-axis 1 unit =0.2ms Y-axis 1div = 10A

FIGURE 24. Current through a motor load of PV-QBC-GZSI-AMD.

VI. CONCLUSION

The suitability of the QBC-GZSIS for induction motor drive that integrates a system has been analyzed in this study. Its quick response makes it suitable for systems that require high stability. The combination of QBC and GZSI is proposed for the control of the induction motor. Simulation results of closed-loop PV-QBC-GZSI-AMD for pumps with different controllers, such as CM-FOPI, CM-PR, and CM-HC, were presented. The settling time for closed-loop PV-QBC-GZSI-AMD is reduced to 3.42 sec using CM-HC. The outcomes illustrate that the closed-loop CM-HC controlled PV-QBC-GZSI-AMD is superior to closed-loop CM-FOPI and CM-PR controllers. However, the drawback of PV-QBC-GZSI-AMD is that it uses a large number of passive elements for QBC and GZSI. The contribution of this work is to identify a controller and to improve the stability of QBC-GZSI-AMD using HC. Additionally, suggestions for future work include implementing silicon carbide devices to enhance the conversion efficiency and investigating the performance of closed-loop PV-QBC-GZSI-AMD with SMC and MPC controllers. This work can be extended for a closed loop QBC-GZSI-AMD system that can be controlled using fuzzy logic / ANN controllers to handle non-linearity due to the Asynchronous motor and QBC-GZSI. The proposed combination of QBC-ZSI is used in the present work controlling a 5 HP asynchronous motor. The studies can be extended to high-power asynchronous motor drives. The viability of using this work for Electric vehicles can be explored in the future.

REFERENCES

[1] A. Hmidet, U. Subramaniam, R. M. Elavarasan, K. Raju, M. Diaz, N. Das, K. Mehmood, A. Karthick, M. Muhibbullah, and O. Boubaker, "Design of efficient off-grid solar photovoltaic water pumping system based on improved fractional open circuit voltage MPPT technique," *Int. J. Photoenergy*, vol. 2021, pp. 1–18, Oct. 2021, doi: 10.1155/2021/4925433.

[2] V. K. Shankar, U. Subramaniam, R. M. Elavarasan, K. Raju, and P. Shanmugam, "Sensorless parameter estimation of VFD based cascade centrifugal pumping system using automatic pump curve adaption method," *Energy Rep.*, vol. 7, pp. 453–466, Nov. 2021, doi: 10.1016/j.egyr.2021.01.002.

[3] B. S. Jebaraj, J. Bennet, R. Kannadasan, M. H. Alsharif, M.-K. Kim, A. A. Aly, and M. H. Ahmed, "Power quality enhancement in electric arc furnace using matrix converter and static VAR compensator," *Electronics*, vol. 10, no. 9, p. 1125, May 2021, doi: 10.3390/electronics10091125.

[4] S. Natarajan, R. Kannadasan, F. Alsaif, and M. H. Alsharif, "Design of novel modified double-ended forward converter for stepper motor drive," *Machines*, vol. 11, no. 8, p. 777, Jul. 2023, doi: 10.3390/machines11080777.

[5] M. N. Uddin, M. R. Islam, and M. A. Matin, "A comparative study on Z-source inverter and conventional inverter fed induction motor drives," in *Proc. 2nd Int. Conf. Electr. Eng. Inf. Commun. Technol. (ICEEICT)*, Dhaka, Bangladesh, 2015, pp. 1–5.

[6] S. Banik, T. K. Saha, and M. A. Motalab, "Quasi Z-source buck-boost inverter fed solar powered water pumping system," in *Proc. 5th Int. Conf. Electr. Eng. Inf. Commun. Technol. (ICEEICT)*, Dhaka, Bangladesh, 2019, pp. 1–6.

[7] A. Arkkio, "Matrix converter applications in pumping systems," *IEEE Trans. Ind. Appl.*, vol. 54, no. 4, pp. 3754–3762, Jul./Aug. 2018.

[8] T. K. Saha, M. A. Motalab, and M. M. Hossain, "Optimal design of PWM inverter fed variable speed water pumping system using hybrid genetic algorithm," in *Proc. 4th Int. Conf. Electr. Eng. Inf. Commun. Technol. (ICEEICT)*, Dhaka, Bangladesh, 2018, pp. 1–5.

[9] A. J. Khan, T. K. Saha, and M. A. Motalab, "A novel quasi Z-source inverter for water pumping system," in *Proc. 4th Int. Conf. Electr. Eng. Inf. Commun. Technol. (ICEEICT)*, Dhaka, Bangladesh, 2018, pp. 1–5.

[10] A. Elmitwally, A. Massoud, and A. Enjeti, "A three-phase Z-source inverter for pumping applications," *IEEE Trans. Ind. Electron.*, vol. 65, no. 1, pp. 307–315, Jan. 2018.

[11] R. S. Sisodia and S. V. Shinde, "A five-level inverter for high-efficiency pumping system," *IEEE Trans. Power Electron.*, vol. 33, no. 3, pp. 2279–2288, Mar. 2018.

[12] A. F. Zobaa, M. I. Taher, A. A. Ibrahim, and A. H. A. Ibrahim, "Nine-switch inverter for efficient pumping system: A comprehensive review," *IEEE Trans. Ind. Electron.*, vol. 65, no. 5, pp. 3809–3819, May 2018.

[13] P. He, H. Xu, J. Liu, and F. Xu, "A direct torque control of permanent magnet synchronous motor for high-efficiency pumping applications," *IEEE Trans. Power Electron.*, vol. 33, no. 11, pp. 9687–9696, Nov. 2018.

[14] Y. Shen, J. Chen, J. Zhang, X. Huang, and J. Wang, "A three-level T-type inverter with reduced size and low THD for pump applications," *IEEE Trans. Ind. Electron.*, vol. 68, no. 2, pp. 1478–1487, Feb. 2021.

[15] Y. Shen, J. Chen, J. Zhang, X. Huang, and J. Wang, "A high-efficiency single-phase T-type inverter with reduced size and low THD for pump applications," *IEEE Trans. Power Electron.*, vol. 36, no. 4, pp. 4148–4157, Apr. 2021.

[16] Z. Yang, Y. Chen, S. Chen, H. Sun, and J. Zhang, "A three-phase dual active bridge inverter for high-efficiency pumping system," *IEEE Trans. Power Electron.*, vol. 36, no. 6, pp. 7059–7070, Jun. 2021.

[17] Z. Yang, Y. Chen, S. Chen, H. Sun, and J. Zhang, "A single-phase dual active bridge inverter for high-efficiency pumping system," *IEEE Trans. Ind. Electron.*, vol. 68, no. 9, pp. 7478–7487, Sep. 2021.

[18] J. Wang, H. Guo, X. Yan, and H. Gao, "A high efficiency single-phase quasi-Z-source inverter for pump applications," *IEEE Trans. Power Electron.*, vol. 35, no. 4, pp. 3824–3834, Apr. 2020.

[19] J. Wang, X. Yan, and H. Guo, "A single-phase zeta inverter for high efficiency pump applications," *IEEE Trans. Ind. Electron.*, vol. 67, no. 1, pp. 472–481, Jan. 2020.

[20] L. P. Pattathurani, S. S. Dash, R. K. Dwibedi, M. D. Raj, R. Kannadasan, M. F. Savio, M. H. Alsharif, and J. H. Kim, "Harmonics minimisation in non-linear grid system using an intelligent hysteresis current controller operated from a solar powered ZETA converter," *Sustainability*, vol. 14, p. 7028, Jun. 2022, doi: 10.3390/su14127028.

[21] H. He, G. Zhu, J. Liu, and Y. Xu, "A single-phase current source inverter with voltage booster for high-efficiency pumping system," *IEEE Trans. Power Electron.*, vol. 35, no. 9, pp. 9358–9368, Sep. 2020.

[22] H. He and Y. Xu, "A high-efficiency three-phase inverter with voltage boosting techniques for pumping system," *IEEE Trans. Ind. Electron.*, vol. 67, no. 9, pp. 7437–7446, Sep. 2020.

[23] S. Y. Wu, C. C. Chuang, and S. Y. Lin, "Single-phase transformerless inverter with modified SVPWM for pump applications," *IEEE Trans. Ind. Electron.*, vol. 66, no. 2, pp. 1058–1068, Feb. 2019.

[24] X. Wang, Q. Jiang, and Y. Liu, "A dual-boost single-phase high-frequency link converter for pump applications," *IEEE Trans. Ind. Electron.*, vol. 66, no. 7, pp. 5223–5233, Jul. 2019.

[25] M. Lu, L. Chen, and X. Wu, "A single-phase high efficiency inverter for water pump application," *IEEE Trans. Ind. Electron.*, vol. 66, no. 5, pp. 4008–4018, May 2019.
[26] J. Zhang, Y. Zhu, and X. He, "A high-efficiency and wide-input-voltage-range pumping inverter based on a capacitor-coupled boost converter," *IEEE Trans. Ind. Electron.*, vol. 66, no. 6, pp. 4795–4805, Jun. 2019.
[27] P. R. Sani, A. Y. Varjani, and R. Gavagsaz-Ghoachani, "An extended coupled-inductor QZS inverter with high-frequency input current ripple suppression," in *Proc. 11th Power Electron., Drive Syst., Technol. Conf. (PEDSTC)*, Feb. 2020, pp. 1–5, doi: 10.1109/PEDSTC49159.2020.9088416.
[28] M. Rajalakshmi, S. Chandramohan, R. Kannadasan, M. H. Alsharif, M. K. Kim, and J. Nebhen, "Design and validation of BAT algorithm-based photovoltaic system using simplified high gain quasi boost inverter," *Energies*, vol. 14, p. 1086, 2021, doi: 10.3390/en14041086.
[29] F. Z. Peng, A. Joseph, J. Wang, M. Shen, L. Chen, Z. Pan, E. Ortiz-Rivera, and Y. Huang, "Z-source inverter for motor drives," *IEEE Trans. Power Electron.*, vol. 20, no. 4, pp. 857–863, Jul. 2005, doi: 10.1109/TPEL.2005.850938.
[30] A. Narendran and R. Sureshkumar, "Hysteresis-controlled–landsman converter based multilevel inverter fed induction-motor system using PIC," *Microprocess. Microsyst.*, vol. 76, Jul. 2020, Art. no. 103099, doi: 10.1016/j.micpro.2020.103099.
[31] R. O. Caceres and I. Barbi, "A boost DC–AC converter: Analysis, design, and experimentation," *IEEE Trans. Power Electron.*, vol. 14, no. 1, pp. 134–141, Jan. 1999.
[32] J. Anderson and F. Z. Peng, "Four quasi-Z-source inverters," in *Proc. IEEE Power Electron. Specialists Conf.*, Jun. 2008, pp. 2743–2749.
[33] M.-K. Nguyen, Y.-C. Lim, and S.-J. Park, "A comparison between single-phase quasi-Z-source and quasi-switched boost inverters," *IEEE Trans. Ind. Electron.*, vol. 62, no. 10, pp. 6336–6344, Oct. 2015.
[34] K. Kim, H. Cha, and H.-G. Kim, "A new single-phase switched-coupled-inductor DC–AC inverter for photovoltaic systems," *IEEE Trans. Power Electron.*, vol. 32, no. 7, pp. 5016–5022, Jul. 2017.
[35] Y. Tang, Y. Bai, J. Kan, and F. Xu, "Improved dual boost inverter with half cycle modulation," *IEEE Trans. Power Electron.*, vol. 32, no. 10, pp. 7543–7552, Oct. 2017.
[36] K. S. R. Kumar, A. Pandian, V. V. Sastry, and D. Raveendhra, "Capacitor clamped coupled inductor bi-directional DC–DC converter with smooth starting," *Machines*, vol. 10, no. 1, p. 47, Jan. 2022.

KRISHNAN SELVARAJ received the B.E. degree in electrical and electronics engineering and the M.E. degree in power electronics and drives from Anna University, Chennai, India, in 2011 and 2013, respectively. He is currently pursuing the Ph.D. degree in electrical and electronics engineering with the Sathyabama Institute of Science and Technology, Chennai. His research interests include converters, inverters, power electronics, and its applications in renewable energy.

G. D. ANBARASI JEBASELVI received the B.E. degree from the Government College of Engineering, Tirunelveli, in 1990, the M.E. degree from the College of Engineering, Guindy, Anna University, in 2003, and the Ph.D. degree from the Sathyabama Institute of Science and Technology, Chennai, India. She is currently working with the Sathyabama Institute of Science and Technology. She has published around 25 articles, including many Scopus-indexed ones, and one of the articles appeared in a high-rated journal viz. Elsevier. Her research findings have been explicit through her paper presentations and publications in various international conferences and journals. Her research interests include renewable energy sources particularly wind and solar systems, modeling of wind electric generators, solar power technologies, and power electronic converters.

MOHAMMED H. ALSHARIF received the B.Eng. degree in electrical engineering (wireless communication and networking) from the Islamic University of Gaza, Palestine, in 2008, and the M.Sc.Eng. and Ph.D. degrees in electrical engineering (wireless communication and networking) from the National University of Malaysia, Malaysia, in 2012 and 2015, respectively. In 2016, he joined the Faculty of the Department of Electrical Engineering, Sejong University, South Korea, as an Assistant Professor, where he has since been promoted to an Associate Professor. His research achievements are reflected in his extensive publication record in top-tier journals in *Electrical and Electronics Engineering*/*Communications Engineering*. His expertise and contributions have also been recognized by leading publishers, such as IEEE, Elsevier, Springer, and MDPI, who has invited him to serve as the guest editor for many special issues. His current research interests include wireless communications and networks, including cutting-edge areas, such as wireless communications, network information theory, the Internet of Things (IoT), green communication, energy-efficient wireless transmission techniques, wireless power transfer, and wireless energy harvesting.

MUN-KYEOM KIM received the Ph.D. degree from the School of Electrical and Computer Engineering, Seoul National University. He is currently a Professor with the School of Energy Systems Engineering, Chung-Ang University, Seoul, South Korea. His research interests include operation techniques in hybrid AC/DC power systems, AI-based smart power networks, big data-based demand response, real-time market design, and multi-agent-based smart city intelligence.